Small-scale multi-axial hybrid simulation of a shear-critical reinforced concrete frame

Vahid Sadeghian[†], Oh-Sung Kwon[‡] and Frank Vecchio[§]

Department of Civil Engineering, University of Toronto, 35 St. George St., Toronto, ON, Canada

Abstract: This study presents a numerical multi-scale simulation framework which is extended to accommodate hybrid simulation (numerical-experimental integration). The framework is enhanced with a standardized data exchange format and connected to a generalized controller interface program which facilitates communication with various types of laboratory equipment and testing configurations. A small-scale experimental program was conducted using a six degree-of-freedom hydraulic testing equipment to verify the proposed framework and provide additional data for small-scale testing of shear-critical reinforced concrete structures. The specimens were tested in a multi-axial hybrid simulation manner under a reversed cyclic loading condition simulating earthquake forces. The physical models were 1/3.23-scale representations of a beam and two columns. A mixed-type modelling technique was employed to analyze the remainder of the structures. The hybrid simulation results were compared against those obtained from a large-scale test and finite element analyses. The study found that if precautions are taken in preparing model materials and if the shear-related mechanisms are accurately considered in the numerical model, small-scale hybrid simulations can adequately simulate the behaviour of shear-critical structures. Although the findings of the study are promising, to draw general conclusions additional test data are required.

1 Introduction

Hybrid simulation is an economical experimental-numerical technique which attempts to realistically assess the behaviour of structures under seismic loads. In most hybrid simulations, displacements of all degrees of freedom are calculated by the main numerical model or simulation framework, and are then imposed on the test specimen(s) and other numerical models at the interface degrees of freedom. The concept of hybrid simulation can equally be applied to the analysis of deficient or deteriorated structures as it can to seismically loaded structures. Most reinforced concrete (RC) structures involve varying degrees of redundancy; as one part of the structure develops cracking or yielding, load may be redistributed to other parts of the structure. As it is impractical to test a model of an entire structure that is deficient, hybrid simulation can be of much value here as well. It will enable the testing of critical components

of a deficient structure, while accounting for the overall structural interactions and load redistributions that may occur. To eliminate limitations associated with large-scale testing (e.g., budget, laboratory space and equipment), the physical model of hybrid simulation can be tested in small-scale; however, care must be taken in preparing the small-scale specimen and in interpreting the results.

To ensure that a small-scale test of an RC specimen represents the response of a full-scale prototype specimen, in addition to imposing appropriate similitude laws, care should be taken to account for scale-related effects at the material-level (Kim *et al*., 1988; Harris & Sabnis, 1999). Many researchers have investigated the accuracy of small-scale test results at the member-level of flexure-critical reinforced concrete structures. The test specimens covered a wide range of member types including 1/12.5-scale models of interior and exterior beam-column joints, an isolated shear wall, and a frame-shear wall system (Wallace & Krawinkler, 1985); 1/6-scale cantilever beam specimens (Kim *et al*., 1988); and 1/2-, 1/3-, and 1/5.5-scale column specimens (Lu *et al*., 1999). In general, the load-deflection responses, crack patterns, and final crack inclinations of small-scale tests correlated well with those obtained from the large-scale tests regardless of the scaling factor, member type,

---

Correspondence to: Vahid Sadeghian, Department of Civil Engineering, University of Toronto, 35 St. George St., Toronto, ON, Canada

    Tel: +1 416-827-6030

    E-mail: vahid.sadeghian@mail.utoronto.ca

[†]PhD Graduate; [‡]Associate Professor; [§]Professor

loading scenario, or testing method. The discrepancies in some of the load-deflection responses were mainly attributed to the dissimilarities between the stress-strain behaviours of the model and prototype materials. In most tests, the reduced-scale specimens exhibited a lower number of cracks with more concentrated damage zones compared to the prototype specimens. However, the rate of reduction in the number of observed cracks reduced as the scaling factor increased. Thus, the distortion in crack spacing had less influence when small-scale tests were compared with medium-scale tests than when medium-scale tests were compared against large-scale tests.

Generally, with reinforced concrete structures, scaling has more pronounced effects on the shear behaviour than on the flexural behaviour. The mechanisms involved in shear behaviour are more complex than flexural behaviour and are related to variables which are sensitive to size effects such as concrete fracture, crack spacing, and aggregate interlock. Several studies demonstrated that the shear stress at failure for concrete members without stirrups decreased as the member size increased (Shioya, 1989; Collins and Kuchma, 1999). However, beams which had minimum shear reinforcement did not show any reduction in shear stress at failure, thus were not sensitive to size effects (Collins and Kuchma, 1999). The minimum required shear reinforcement was defined according the Canadian Standard Association for the "Design of Concrete Structures" (CSA-A23.3, 2014). Other researchers performed similar studies on other types of shear-critical members (i.e., failure predominantly occurs due to shear mechanisms) such as columns (McDaniel *et al.*, 1997; Ohtaki, 2000) and shear walls (Ghorbani-Renani *et al.*, 2009). All the specimens contained the minimum shear reinforcement as specified by CSA-A23.3. Based on the test results, almost all the small-scale specimens accurately simulated the prototype behaviour. The shear strength degradation of large-scale specimens started at earlier load stages than the scaled specimens. As with flexure-critical members, as the scale of the specimen reduced, fewer cracks with wider spacing were observed.

In recent years, application of hybrid simulation to small-scale testing was the focus of a few research studies. Holub (2009) tested a reinforced concrete bridge structure in a hybrid simulation manner. The physical model represented a 1/10-scale of one of the piers. Gencturk and Hosseini (2015) performed a similar study on 1/8-scale columns. Saouma *et al.* (2014) conducted a real-time hybrid simulation of a non-ductile reinforced concrete frame and compared the results with those obtained from a shake table test. The test specimen was a 1/3-scale representation of one of the flexure-shear-critical columns. For all of the aforementioned hybrid simulations the numerical model was analyzed using

fibre beam elements. In general, the response obtained from the small-scale tests agreed well with the large-scale experimental results. More cracking and damage was observed in the large-scale tests. Discrepancies between some of the results were mainly attributed to differences at the material-level and deficiencies of the frame-type analysis (i.e., frame elements with plastic hinges and layered frame elements) in accurately capturing the shear deformations and behaviour at the disturbed regions.

One effective method to assess the performance of a structure under seismic loads is to impose a component of the actual ground motion on the test specimen or use a time integration technique to numerically consider the dynamic effects. Another popular and practical method to simulate a seismic event that does not require dynamic loading equipment, is to test the specimen in a quasi-static manner under a reversed cyclic loading condition. Although quasi-static testing cannot take into account some of the dynamic effects (e.g., inertia, mass, and damping), it can be used to gain valuable insight on the failure mode, ductility, and energy dissipation of a structure which are key parameters in predicting the structural behaviour in a seismic event. The effectiveness of quasi-static testing becomes more apparent as structural codes move toward the performance-based design approach, in which the main objective is to meet a specific set of performance requirements such as damage levels and ductility demands.

In this study, a recently developed multi-scale framework, Cyrus (Sadeghian *et al.*, under review), was further extended to combine numerical models with experimental components to accommodate hybrid testing. A small-scale experimental program was conducted using a multi-axial hydraulic testing equipment under a reversed cyclic loading condition to verify the proposed hybrid simulation framework. The experimental program comprised of three parts: 1) the hybrid simulation proof tests of two steel frame structures within the linear elastic range, 2) the hybrid simulation tests of two reinforced concrete frame structures with different failure modes, and 3) the hybrid simulation test of a shear-critical reinforced concrete frame that had been previously tested as a full-frame specimen in a quasi-static manner. The physical models were 1/3.23-scale representations of the critical members of the structures. The remainder of the structures were analyzed by integrating two programs; a frame-type analysis program (non-critical members) and a detailed finite element analysis program (critical members). The hybrid simulation results were compared against those obtained from a large-scale test previously conducted in a conventional manner and from stand-alone numerical models.

2   Configuration of hybrid simulation framework and verification tests

2.1 Hybrid simulation framework

The proposed multi-scale framework Cyrus (Sadeghian *et al.*, under review), which was primarily developed to integrate various types of numerical models, was further extended to enable hybrid testing. To establish communication between the actuator controller and simulation framework, a generalized controller interface program named the Network Interface for Controllers (NICON) (Zhan and Kwon, 2015) was used. NICON is applicable to a wide range of test configurations with different specimen orientations, control point positions, or number of interface degrees of freedom (DOFs) and actuators. The communication between NICON and actuator controller was established through analog I/O (i.e., input/output) signals using the National Instruments CompactRIO hardware. A NI hardware box was assembled which contained a high performance real-time controller (NI cRIO-9022) and two input and output analog modules (NI 9205 and NI 9264, respectively). To control the 6-DOF hydraulic testing equipment, six channels of command outputs to the controller (displacements) and twelve channels of measured inputs from the controller (displacements and reaction forces) were established. Also, four additional input channels were placed to record external measurements. To facilitate addition of other potential numerical or physical modules to the simulation framework, a recently developed standardized data exchange format and communication protocol called the University of Toronto Networking Protocol (UTNP) (Huang *et al.*, 2015) was employed.

For multi-axial hybrid simulation, multiple actuators are used to control coupled DOFs of a specimen (e.g., a member under axial and lateral forces and moment). The displacement commands received from the simulation framework are in the Cartesian coordinate system of the numerical model and should be transformed to the loading platform coordinate system and then the actuator strokes. Also, the measured displacements and forces from the actuators should be converted back to the loading platform coordinate system and then the Cartesian coordinate system of the numerical model. In this study, the coordinate transformations were performed according to an iterative approach developed by Nakata *et al.* (2010) in the NICON interface program. The procedure is based on the Newton-Raphson method and takes into account the geometric nonlinearity of the test setup.

Hybrid simulation was conducted based on the Modified Newton Raphson procedure implemented in the Cyrus simulation framework. Because dynamic effects were not considered in this study, a numerical time integration scheme was not required. Several iterations were performed at each load stage to fulfill the compatibility and equilibrium requirements between the test specimen and numerical models. The hybrid test was conducted in a quasi-static manner with sufficiently small load step increment to minimize the damage on the specimen due to iterations performed at each load stage. The actuators were controlled with a closed loop PID controller, but the test was an open loop test; i.e., the measured response was not fed back to change the control command. To reduce the communication data between the simulation framework and numerical models, only the equivalent restoring forces and displacements at the interface DOFs were transferred. The equivalent values were computed by performing a static condensation procedure which eliminated the displacements and forces of the internal DOFs. Unbalanced forces resulting from the nonlinear behaviour of the test specimen were calculated based on the initial stiffness and measured force reactions. The initial stiffness of each test specimen was estimated using the measured elastic modulus of the related microconcrete. The initial stiffness was increased by 10% to avoid underestimating the actual stiffness of the specimen and divergence of the nonlinear solution. The initial stiffness estimation was deemed reasonable since no fluctuation was observed in the measured reactions and load-deflection response of the system. The accuracy of the imposed displacements at the specimen control point and the potential relative deformations of the concrete end blocks with respect to the end steel plates were monitored using a 3D scanner and external LED targets. Figure 1 shows an overview of the hybrid simulation configuration.

2.2 Test setup

As shown in Fig. 2, a 6-DOF hydraulic testing facility which is equipped with three actuators in the horizontal direction (two actuators in the X direction and one actuator in the Y direction) and three actuators in the vertical direction (the Z direction) was assembled as the loading platform. The strokes of the horizontal and vertical actuators are 76.2 mm and 50.8 mm, respectively. Each actuator has a force capacity of 14.7 kN. The actuators are attached to a testing table with dimensions of 762 mm × 762 mm × 99 mm. The specimen and actuators are supported against a stiff steel frame. The clearance between the supporting beam and the testing table can be adjusted according to the length of the specimen.

2.3 Numerical components

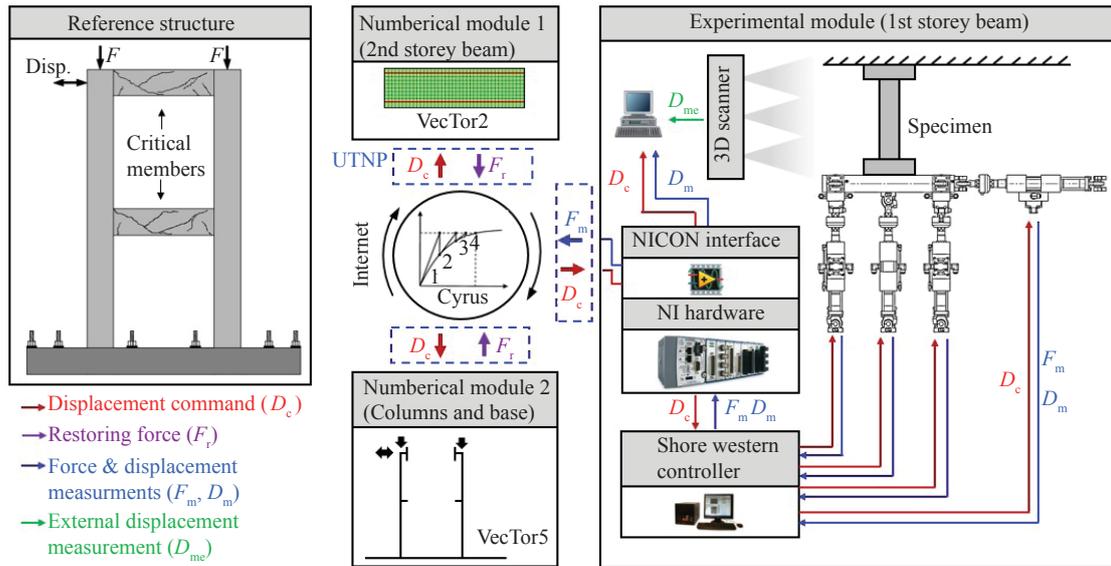In hybrid simulation, the numerical substructures are modelled in full-scale while the physical substructures
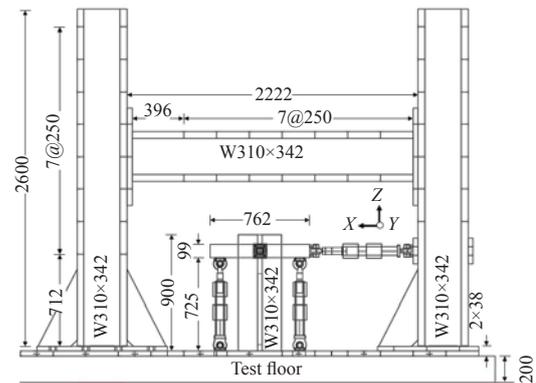
Fig. 1   Overview of hybrid simulation configuration

Fig. 2   Details of 6-DOF loading platform (dimensions in millimeters)

may be constructed in reduced-scale with scaling factors determined according to the available laboratory equipment. To integrate the numerical substructures with physical substructures in different scales, the input and output of each component should be properly scaled according to its scaling factor and similitude laws. For a quasi-static hybrid test, the translational displacements computed by the simulation framework should be scaled with a length scale factor (S) prior to applying to the physical specimens. Similarly, the reaction forces and translational displacements measured from the physical components should be scaled using force and moment scale factors (S^2 and S^3) and a length scale factor (S), respectively, prior to sending them to the numerical models. It should be noted that the computed and measured rotational displacements do not require scaling.

The numerical models in most of the previously reported small-scale hybrid simulations were analyzed using a frame-type software. Although this type of analysis is computationally efficient, it is based on

the assumption of "plane section remains plane", compromising its ability to capture the detailed behaviour of the structure, particularly for shear-critical members in which accurate consideration of shear deformations, shear slip along the cracks, and stresses at the disturbed regions are crucial. In this study, a mixed-type analysis approach was employed to accurately analyze the numerical substructure in a computationally efficient manner. The potentially critical components of the numerical substructure were modelled in a finite element program, VecTor2 (Wong et al., 2013), while the non-critical members were modelled in a frame-type analysis program, VecTor5 (Guner and Vecchio, 2011). The newly developed F2M interface elements (Sadeghian et al., 2017) were used to connect the two sub-models. VecTor2 have been successfully employed for analyzing various types of reinforced concrete structures over the last two decades (e.g., Collins et al., 1997; Vecchio, 2002). Using a detailed finite element program enabled the consideration of shear deformations and accounting for second-order material effects such

as tension stiffening, tension softening, compression softening, and shear slip along crack surfaces. In Section 2.3.1 and 2.3.2, the models used for the second-order material effects, which were found to be important in capturing the behaviour of shear-critical members in hybrid simulations, are presented.

2.3.1 Tension softening

Lightly reinforced concrete members experience a brittle type of failure under tensile stresses resulting from shear loads. However, the failure is not instantaneous and requires cracks to develop and propagate. Therefore, instead of an abrupt drop to zero stress in the post-peak response, there is a gradual reduction in strength known as tension softening. As shown in Fig. 3, a bilinear tension softening model, adopted from CEB-FIP (1990), was employed. The formulations of the model are presented in Eq. (1) and Eq. (2)

Fig. 3 Concrete tension softening model

$$
f_{c1} = \begin{cases} f_{cr}\left[1 - 0.80\left(\dfrac{\varepsilon_{c1} - \varepsilon_{cr}}{\varepsilon_{ch3} - \varepsilon_{cr}}\right)\right] & \varepsilon_{c1} < \varepsilon_{ch3} \\[3mm] 0.2 f_{cr}\left[1 - \left(\dfrac{\varepsilon_{c1} - \varepsilon_{ch3}}{\varepsilon_{ch4} - \varepsilon_{ch3}}\right)\right] & \varepsilon_{ch3} \le \varepsilon_{c1} < \varepsilon_{ch4} \\[3mm] 0 & \varepsilon_{ch4} \le \varepsilon_{c1} \end{cases}
$$
(1)

$$
\varepsilon_{ch3} = 0.64\left(\frac{G_f}{L_f f_{cr}}\right) + \varepsilon_{cr}; \quad \varepsilon_{ch4} = 6.8\left(\frac{G_f}{L_f f_{cr}}\right) + \varepsilon_{cr} \quad (2)
$$

where f_{cr} and ε_{cr} are the cracking stress and strain, f_{c1} and ε_{c1} are the concrete stress and strain in the principal directions, G_f is the fracture energy (i.e., the energy required to form a complete crack of unit area) which describes the resistance of the concrete to cracking and is equivalent to the area beneath a graph of tensile stress versus crack width, L_f is the representative length (i.e., the distance over which the crack is assumed to be uniformly distributed) which is equal to half of the crack spacing, ε_{ch3} is the strain at 20 percent of the cracking stress, and ε_{ch4} is the ultimate strain.

2.3.2 Local conditions at the crack

The local conditions at the crack were considered according to the Disturbed Stress Field Model (DSFM) (Vecchio, 2000). Based on this model, the concrete tensile stresses (f_{c1}) are nearly zero at the crack locations; however, concrete can carry tensile stresses between the cracks due to tension stiffening effects. Compensating for the reduction in concrete stresses at the crack requires an increase in reinforcement stresses (f_{scri}) locally to satisfy equilibrium. The increase in reinforcement stresses develop shear stresses (v_{ci}) on the crack surface to balance forces in the principal 2 direction (see Fig. 4). The slip deformations caused by shear stresses across the crack are incorporated into the compatibility relations of the DSFM model. The equilibrium equations for local
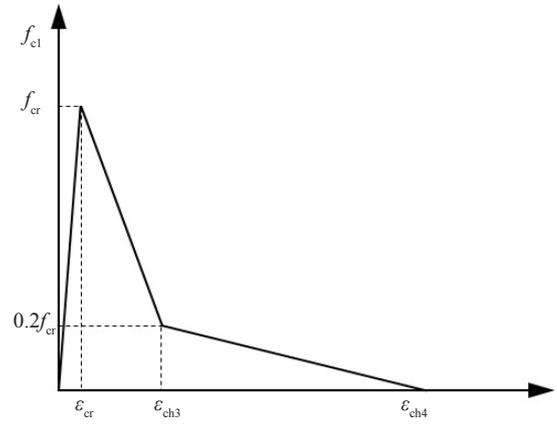
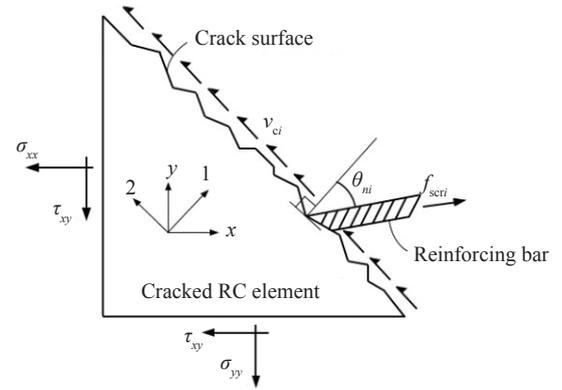reinforcement stresses and concrete shear stresses at the crack are given in Eq. (3) and Eq. (4).

Fig. 4 Stress conditions at the crack

$$
f_{c1} = \sum_{i=1}^{n} \rho_i \left(f_{scri} - f_{si}\right)\cos^2\theta_{ni} \tag{3}
$$

$$
v_{ci} = \sum_{i=1}^{n} \rho_i \left(f_{scri} - f_{si}\right)\cos\theta_{ni}\sin\theta_{ni} \tag{4}
$$

where ρ_i is the reinforcement ratio of the ith reinforcing bar, θ_{ni} is the angle between the principal 1 direction and the ith reinforcing bar direction, and f_{si} is the average stress in the ith reinforcing bar.

2.4 Verification tests

To verify the performance of the hybrid simulation framework, two steel frame structures (Frame 1 and Frame 2) were tested within the linear elastic range in a quasi-static hybrid manner. The steel frames had similar structural configurations as the reinforced concrete frames planned to be tested. Details of Frame 1 and Frame 2 are shown in Fig. 5(a). Frame 1 was a one-span one-storey structure in which the left column was considered the experimental component and was placed in the test setup
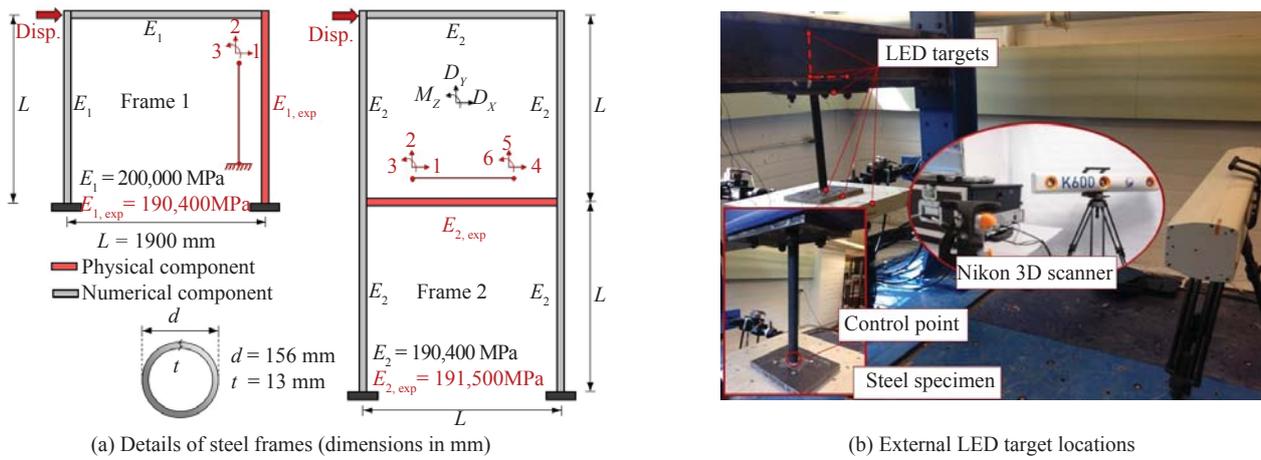
(a) Details of steel frames (dimensions in mm)

(b) External LED target locations

Fig. 5   Hybrid simulation of steel frame structures

upside down. Translational and rotational displacements at the top end of the column specimen were controlled as the interface DOFs between the numerical and physical substructures while the bottom end was assumed to be fixed. Frame 2 was a one-span two-storey structure in which the lower storey beam was selected as the test specimen. The beam specimen consisted of two interface nodes each with two translational and a rotational DOFs. To control displacements at the two ends of the beam specimen, relative deformations were computed based on rigid body motion and were applied to one end of the specimen while the other end was considered to be fixed. In both structures, the test specimen was a 1/3.25-scale representation of the prototype member. The remainder of the frames were modelled using beam elements in the VecTor5 analysis software. The external load was applied by controlling the lateral displacement of the left joint node in a quasi-static reversed cyclic manner. Cyrus combined the numerical and physical substructures. The displacements of the specimen at the control point and potential relative movements of the steel plates with respect to the top support beam and hydraulic

testing platform, were externally monitored with a three-dimensional coordinate scanning system (Nikon K-Series Optical CMM). The scanner continuously recorded the coordinates of the LED targets attached to the specimen, testing table, and supporting frame.

The scaled forces and moments at the interface node between the numerical and physical substructures were compared against the linear elastic analysis results in Fig. 6. It can be seen that the results from hybrid simulation agreed well with the linear elastic analysis responses. The discrepancies in the axial forces (F2 for Frame 1 and F4 for Frame 2) were attributed to the low levels of axial displacements compared to the transverse displacements and rotations applied to the test specimen (for example with frame 1: $D_{X,\max} = 2.5$ mm, $D_{Y,\max} = 0.02$ mm, and $\theta_{Z,\max} = 0.0023$ rad). The axial displacements were smaller than the tolerance of the testing equipment and therefore it was not practical to accurately control this displacement component at such low levels. For the comparison between the numerical and physical values of the translational and rotational displacements at the interface node refer to Sadeghian (2017).
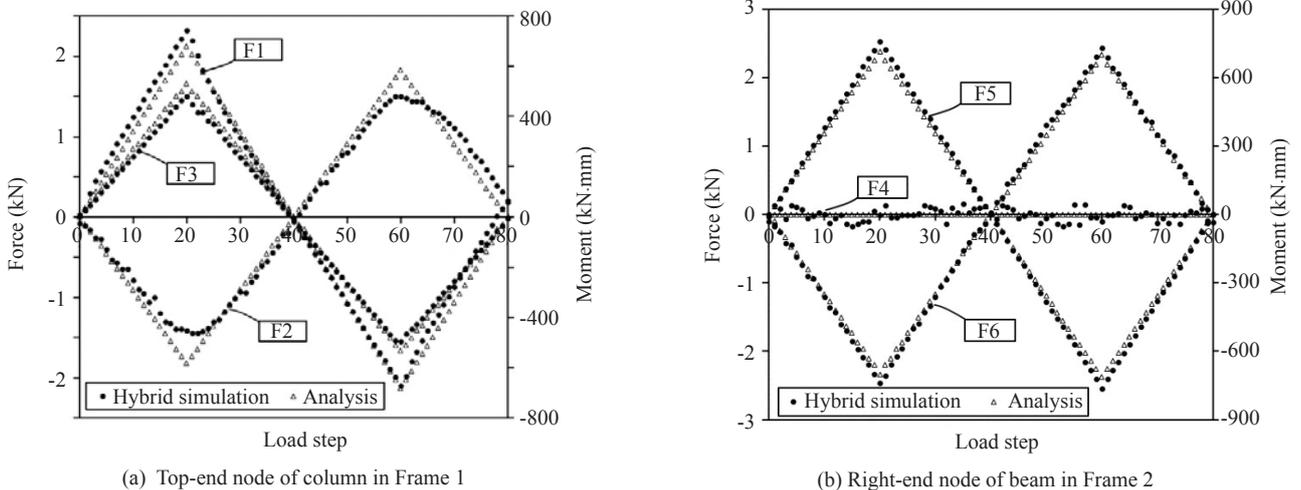

(a) Top-end node of column in Frame 1

(b) Right-end node of beam in Frame 2

Fig. 6   Scaled forces and moments at the interface node of steel frames

3 RC frames with critical columns

3.1 Reference structures

Two one-storey one-bay reinforced concrete frame structures with critical columns were tested under a quasi-static reversed cyclic loading condition. The test variable was the amount of shear reinforcement in the columns. The first frame was designed to exhibit a ductile behaviour containing adequate transverse reinforcement ($\rho_v = 0.4\%$) while the other frame was designed to be shear-critical with a low amount of transverse reinforcement ($\rho_v = 0.1\%$) which was slightly higher than the minimum requirement specified by CSA-A23.3. To conduct hybrid simulations on each frame, one of the columns was considered as the test specimen and the rest of the structure was modelled using nonlinear VecTor analysis programs. The test specimens were a 1/3.23-scale model of the prototype columns. The external load was applied as a lateral displacement at the mid-depth of the beam in a reversed cyclic manner. Cyrus was used to integrate the numerical and physical substructures. Details of the two frame structures, loading patterns, and material

properties are presented in Fig. 7, Fig. 8, and Table 1, respectively.

3.2 Material tests

To properly replicate the actual response of a reinforced concrete member in small-scale, the material properties of the scale model should be similar to that exhibited by the prototype structure. In particular, the stress-strain responses of the concrete and steel in tension and compression and bond-slip effects resulting from the interaction between the material components should be accurately represented in the reduced-scale tests. In this study, the prototype structure was a shear-critical frame (Duong *et al*., 2007) previously tested in large-scale as a full-frame specimen at the University of Toronto. The model materials were a 1/3.23-scale representation of the prototype concrete and reinforcing bars.

For the microconcrete, the maximum size of aggregates was scaled to fulfill similitude requirements. The maximum aggregate sizes (a_{max}) of 3.36 mm (US No. 6 sieve) and 4.00 mm (US No. 5 sieve) were used for the small-scale specimens of the two-storey frame ($a_{max, org} =$
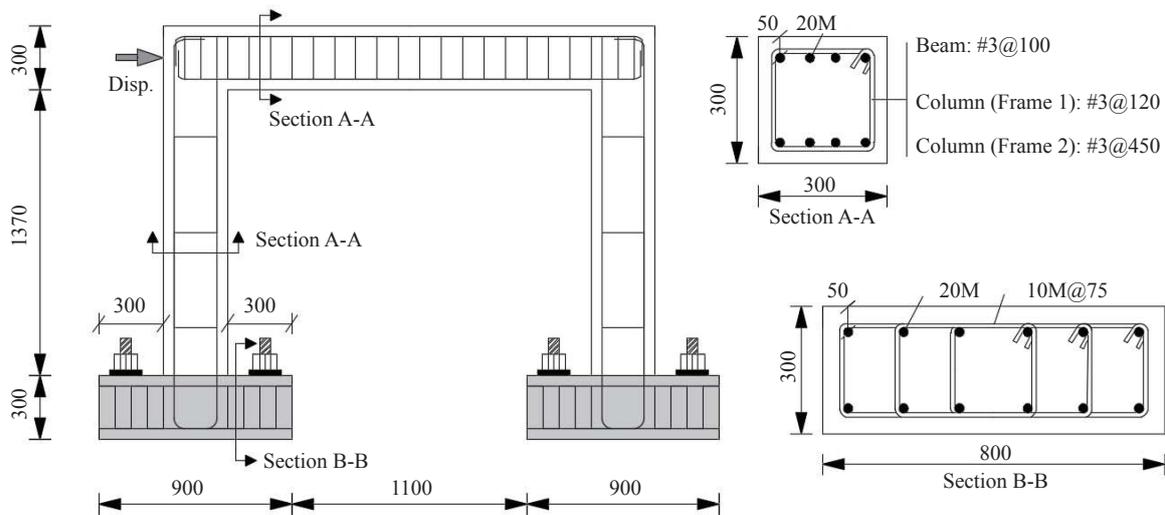

Fig. 7 Details of shear-critical and flexure-critical frames (dimensions in mm)
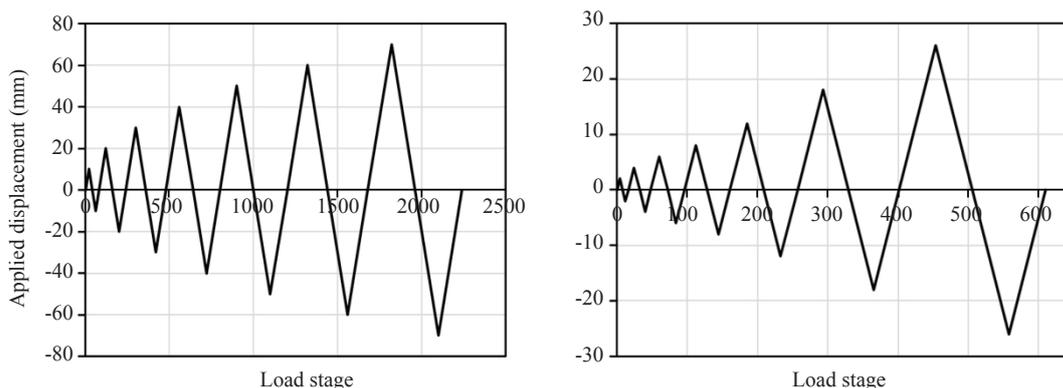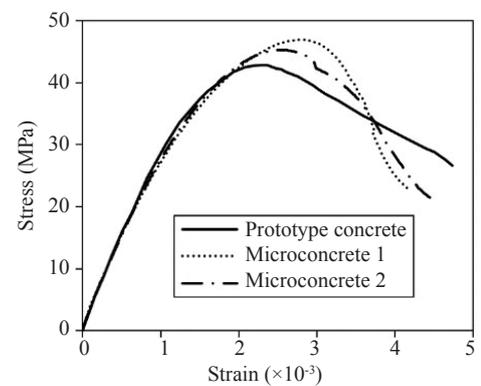

Fig. 8 Loading protocol: flexure-critical frame (left) and shear-critical frame (right)
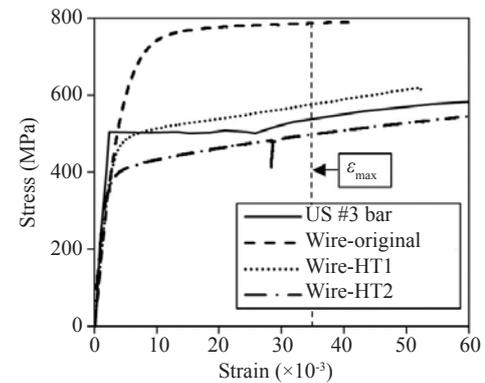
Table 1 Material properties of frame structures

Concrete			
Member Type	f'_c (MPa)	$\varepsilon_0 (\times 10^{-3})$	Max agg. size (mm)
Beam	42.9	2.31	14
Column & Foundation	46.9	2.78	14

Reinforcement						
Member Type	Bar Size	Diameter (mm)	Area (mm²)	f_y (MPa)	E_s (MPa)	f_u (MPa)	ε_u ($\times 10^{-3}$)
Beam	20M	20.0	300	447	198,400	603	130
	US #3	9.5	71	506	210,000	615	120
Column & Foundation	10M	10.0	100	400	200,000	600	100
	20M	20.0	300	503	194,000	543	57
	US #3	9.5	71	498	181,000	620	52

10 mm) in Duong *et al.* (2007), which will be denoted as the Duong frame hereafter, and one-storey frames ($a_{max, org}$ = 14 mm), respectively. The compressive stress-strain relationship of a model concrete was considered the most important property of the material that needed to be replicated (Harris and Sabnis, 1999). Typically, for a specific compressive strength, microconcrete tends to overestimate the compressive strains and tensile strength compared to a similar prototype concrete (Noor and Wijayasri, 1982). To compensate for the softer compressive behaviour and higher tensile strength of the microconcrete, the minimum size of aggregate was restricted to 0.297 mm (US No. 50 sieve). Also, a much higher coarse-to-fine particle ratio was used to reduce the aggregate surface area and avoid excessive tensile strength. In the trial mix designs, the aggregate content was increased to compensate for the low modulus of elasticity of microconcrete since the aggregate has higher stiffness than the cement paste. Six trial batches were cast in standard size cylinders (100 mm × 200 mm), and tested under uniaxial compression in 14 days. The influence of four parameters were investigated: water-to-cement ratio (W/C), aggregate-to-cement ratio (A/C), aggregate gradation, and maturity level of the microconcrete. Type III Portland cement was employed to accelerate the testing process. Figure 9(a) compares the average stress-strain responses of the final two microconcrete mix designs, obtained from testing three cylinders, with the prototype concrete behaviour reported in Duong *et al.* (2007). It can be observed that the behaviour of microconcrete is close to that of the prototype concrete. Thus, Microconcrete 1 and Microconcrete 2 were used for the small-scale specimens of the one-storey frames and the Duong frame, respectively. Since the concrete tensile strength of the Duong frame at the time of testing was not reported, no tensile test was conducted on the model concrete.
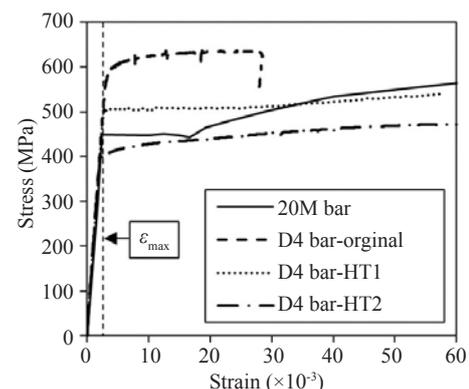
The lower storey beam of the Duong frame was represented as a test specimen in the hybrid simulation.

(a) Model concrete

(b) Model transverse reinforcement

(c) Model longitudinal reinforcement

Fig. 9 Average stress-strain responses of the model materials

The beam contained two types of reinforcements; #3 US bars and 20M bars were used for the transverse reinforcement and the longitudinal reinforcement, respectively. The reinforcement dimensions of the small-scale specimens were scaled according to the similitude requirements. For the transverse reinforcement, using smooth wires was deemed acceptable since bond-slip effects are typically insignificant in stirrups. The wires were made of 316L stainless steel material and had a nominal diameter of 3.175 mm which was the closest available diameter of wires to represent the scaled reinforcing bars. A heat treatment process was carried out on six batches of wires to manipulate the behaviour of model reinforcement to match the prototype response. Temperatures ranging from 843 °C to 1015 °C were investigated using a heating time of 20 minutes. To ensure the wires were exposed to a uniform temperature and had similar material properties, three tensile tests were performed on each batch. The average stress versus strain responses of the final selected batches are compared against the prototype US #3 bar behaviour in Fig. 9(b). The maximum strain in the beam transverse reinforcement computed from the nonlinear analysis of the frame is also shown on the graph ($\varepsilon_{max} = 35 \times 10^{-3}$ mm/mm). Based on the test results, Wire-HT1 (heat treated at 871 °C) and Wire-HT2 (heat treated at 899 °C) were employed as the transverse reinforcement for the scaled hybrid test specimens of the one-storey frames and the Duong frame, respectively.

Unlike with transverse reinforcement, for the longitudinal reinforcement the bond between the reinforcing bar and concrete can significantly influence the behaviour of the structure. To properly simulate the bond characteristics in small-scale, D4 deformed bars with 5.72 mm nominal diameter were used as the model longitudinal reinforcement. Similar to the model transverse reinforcement, five batches of reinforcing bars were heat treated with temperatures ranging from 538 °C to 671 °C and heating times of 1.5 hours to 3.0 hours. The average stress versus strain responses of the final selected batches are compared against the prototype 20M bar behaviour in Fig. 9(c). It is worth noting that according to the full-frame test results, the beam longitudinal reinforcement experienced a maximum strain of 3.3×10^{-3} mm/mm which was slightly higher than the yielding strain value (2.25×10^{-3} mm/mm). According to the test results, D4 Bar-HT1 (subjected to temperature of 565 °C for 2 hours) and D4 Bar-HT2 (subjected to temperature of 621 °C for 2 hours) were selected as the longitudinal reinforcement for the test specimens of the one-storey frames and the Duong frame, respectively.

3.3 Physical specimen of hybrid tests

Two I-shaped reusable wooden formworks were constructed, each comprised of two end blocks with

dimensions of 250 mm × 250 mm × 90 mm and a test region with dimensions of 424 mm × 93 mm × 93 mm. The specimen contained four D4 bars as the top and bottom longitudinal reinforcement and 3 (shear-critical frame) and 10 (flexure-critical frame) wire stirrups as the transverse reinforcement. Figure 10 shows details of the specimen. To model the anchorage of the longitudinal reinforcement, both ends of the D4 bars were threaded and screwed to two 12.7 mm thick end steel plates. To prevent the wires from premature opening, each end was bent 180 degrees and fixed with small tie wires. Including the end blocks was deemed necessary for realistic simulation of the stress distributions at the top and bottom parts of the test region. To avoid cracking and failure in the end blocks, they were heavily reinforced in the longitudinal and transverse directions using D4 bars. Also, the top and bottom steel plates and 12.7 mm diameter threaded rods provided additional confinement and strength for the end blocks. Twelve threaded rods (eight at the bottom and four at the top) were used to bolt the specimen to the top and bottom steel plates of the test setup. To enable attachment of the specimen to the table, the threaded rods in the end blocks were covered by thin copper pipes that were cast-in-place. The specimens were tested 14 days after casting the concrete.
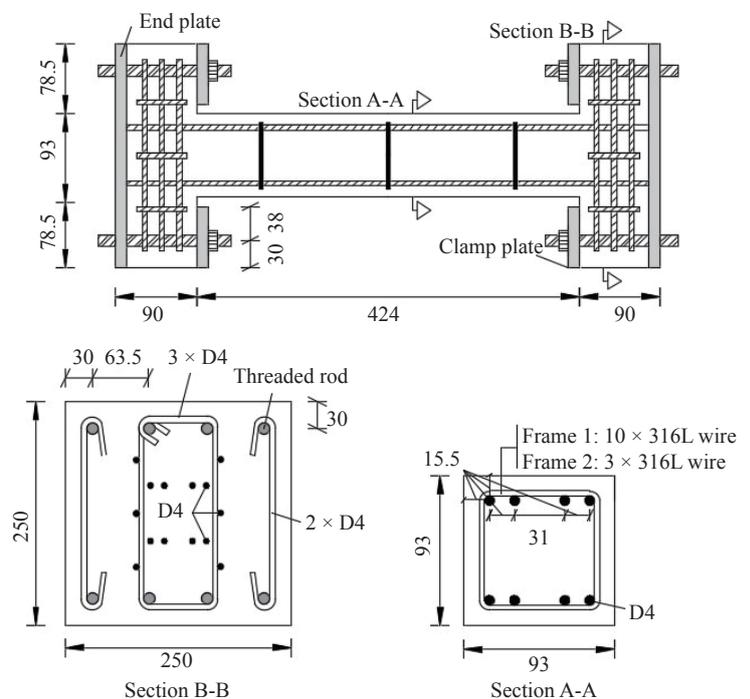

Fig. 10 Details of small-scale column specimen (dimensions in mm)

3.4 Numerical models

Two finite element models were created for each structure: 1) a substructure model including the beam and right column for hybrid simulation and 2) a full-

frame model for mixed-type analysis. Figure 11 shows the numerical and physical substructures for hybrid simulation. The beam was modelled in VecTor5 while the right-side column, the critical member of the numerical substructure, was simulated in VecTor2. The VecTor5 sub-model was comprised of 12 fibre beam elements of approximately 200 mm length. Each frame element was divided into 30 concrete layers, enabling accurate analysis through the section. Based on the stirrups details presented in Fig. 7, the out-of-plane and transverse reinforcement ratios were determined and assigned to the outer and core layers of the cross section, respectively. The joint panels were modelled with stiffened elements to avoid premature failure. The amounts of the longitudinal and transverse reinforcement of the stiffened elements were increased by a factor of two to avoid artificial damage as suggested by Guner and Vecchio (2011). To model the external load, the lateral displacement of the left joint node was controlled in a reversed cyclic manner with 0.5 mm increments.

For the VecTor2 sub-model, the right-side column, including the base foundation, was modelled with 662 concrete rectangular elements and 144 steel truss elements. A mesh size of 60 mm × 60 mm was used for the heavily reinforced base foundation while the columns were modelled using a finer mesh size of 25 mm in the horizontal direction by 30 mm in the vertical direction. The longitudinal reinforcement was represented with truss elements. The transverse reinforcement was added as a smeared component to the rectangular concrete elements. To provide a fixed end condition for the frame, all the nodes located at the bottom row of the foundation were fully restrained in both the X and Y translational directions. For the full-frame model, the test specimen was numerically modelled and had identical details as the right-side column.
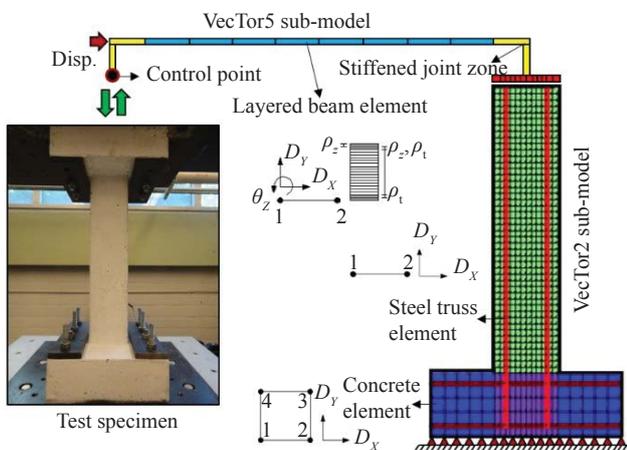

Fig. 11 Numerical and physical substructures for hybrid simulation

3.5 Results and discussion

The load-deflection responses obtained from the small-scale hybrid tests are compared against the finite element analysis results of the prototype structures in Fig. 12. For both the flexure-critical and shear-critical frames, the overall response obtained from the hybrid simulation agreed well with that computed by the stand-alone analysis. The hybrid tests had a tendency to underestimate the stiffness and peak loads of the initial loading cycles compared to the stand-alone analyses. This was primarily attributed to the lower stiffness of the microconcrete (E_c = 29,300 MPa obtained from material tests) compared to the prototype concrete (E_c = 31,800 MPa computed based on the Hognestad (1951) model). For the flexure-critical frame, the energy dissipation (i.e., area under the load-deflection curve) of the analysis and hybrid test correlated reasonably well; however, for the shear-critical frame the analysis resulted in a lower energy dissipation than the test, mainly due to the lower computed plastic offsets (i.e., permanent deformations under cyclic loading), particularly in the last two loading cycles.

As expected, the flexure-critical frame exhibited a ductile behaviour with failure occurring at lateral displacements of 60 mm for the hybrid test and 63 mm for the analysis. Conversely, the shear-critical frame response was brittle with strength decay initiating at displacements of 17.5 mm for the hybrid test and 12 mm for the analysis. For the shear-critical frame, the strength degradation of the hybrid test initiated at later load stages and was more gradual compared to the analysis. Figure 13 compares the hybrid simulation responses of the two frames. It can be seen that addition of more stirrups increased the ultimate strength and ductility of the frame by 32% and 243%, respectively.

Based on the stand-alone analysis results of the flexure-critical frame, the yielding of the longitudinal reinforcement and transverse reinforcement initiated at the base of the column in the second and third loading cycles, respectively. From the fifth loading cycle, the concrete elements located at the toe of the column started to reach the crushing strength. For the shear-critical frame, however, the maximum computed stress in the longitudinal reinforcement was below yielding ($0.89f_y$). Also, yielding of the stirrups and crushing of concrete elements initiated at much lower ductility levels (6 mm and 12 mm, respectively) compared to the flexure-critical frame.

The crack patterns obtained from the test and analysis at the peak load stage of the final cycle are presented in Fig. 14. It can be seen that for both structures the crack pattern of the hybrid test correlated reasonably well with that computed by the analysis. For the flexure-critical
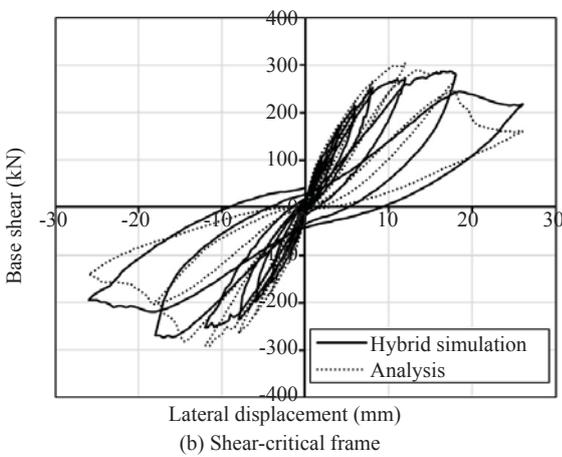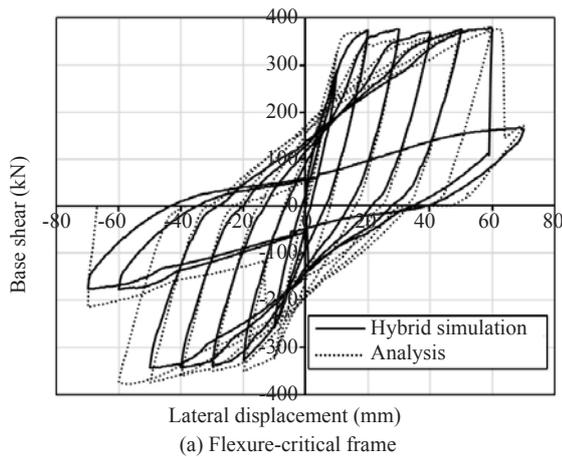
(a) Flexure-critical frame

(b) Shear-critical frame

Fig. 12 Load-deflection responses for frames with critical-columns
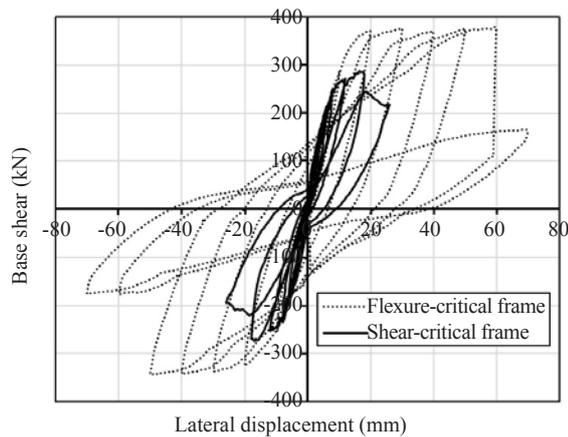

Fig. 13 Comparison between flexure-critical frame and shear-critical frame hybrid simulation responses

frame, the primary crack which ultimately caused the failure of the test specimen developed in the horizontal direction along the base of the column. Two minor flexural cracks with approximately 80 mm spacing from the base were also observed. In addition to flexural cracks, the specimen experienced two small diagonal shear cracks extending from the base to about the mid-height of the specimen in the opposite direction. A similar crack pattern was computed by the analysis. The first eight rows of the elements at the base demonstrated large

flexural cracks. These cracks were accompanied by two diagonal shear cracks which continued as vertical cracks along the longitudinal reinforcement layers. The lower number of flexural cracks and the highly concentrated damage zone observed in the small-scale specimen were in line with the findings of most previous small-scale tests reported in the literature.

For the shear-critical frame, both the test and analysis exhibited two large diagonal shear cracks, in a cruciform shape at each end of the column, which then continued as a sliding crack along the longitudinal reinforcement layers. The specimen experienced a brittle type of failure due to sudden opening of the shear and sliding cracks, matching the behaviour obtained from the analysis. The shear crack development in the analysis initiated at an earlier load stage compared to the small-scale specimen. A similar behaviour was observed in the shear-critical reinforced concrete model columns tested by Ohtaki (2000).
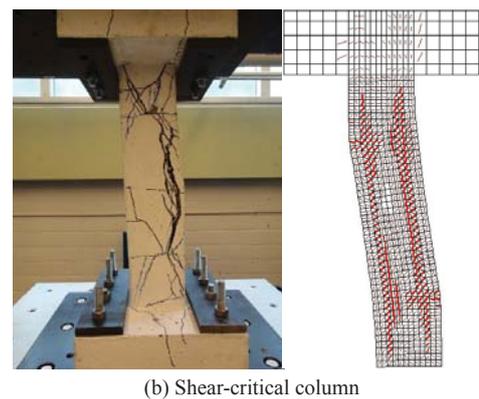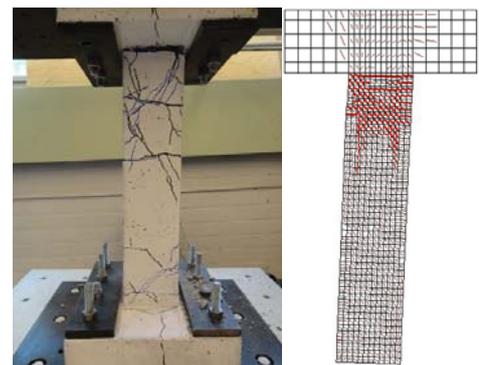

(a) Flexure-critical column

(b) Shear-critical column

Fig. 14 Crack patterns at the final loading cycle for the flexure-critical frame (a) and shear-critical frame (b)

4 RC frame with shear-critical beams

4.1 Reference structure

In 2007, an experimental study was conducted at the University of Toronto to assess the behaviour of a shear-critical reinforced concrete frame under simulated seismic loads (Duong *et al*., 2007). A one-bay two-storey

frame with inadequate shear reinforcement in the beams was tested under a constant axial load and a reversed cyclic lateral displacement in a quasi-static manner. The test reported large shear cracks in both the first-storey and second-storey beams. In this study, the behaviour of the frame was re-examined in small-scale using the multi-axial hybrid simulation technique.

Details of the frame are shown in Fig. 15. An axial load of 420 kN was imposed on each column and maintained constant during the test in a force-controlled manner. The lateral load was applied in a displacement-controlled manner at the mid-depth of the second-storey beam. The transverse reinforcement ratio of the columns ($\rho_v = 1.02\%$) was markedly higher than the respective value of the beams ($\rho_v = 0.16\%$). It is worth noting that the minimum shear reinforcement ratio of the section required by the CSA-A23.3 was 0.08%. Table 2 presents the concrete and reinforcement material properties reported in the original test.
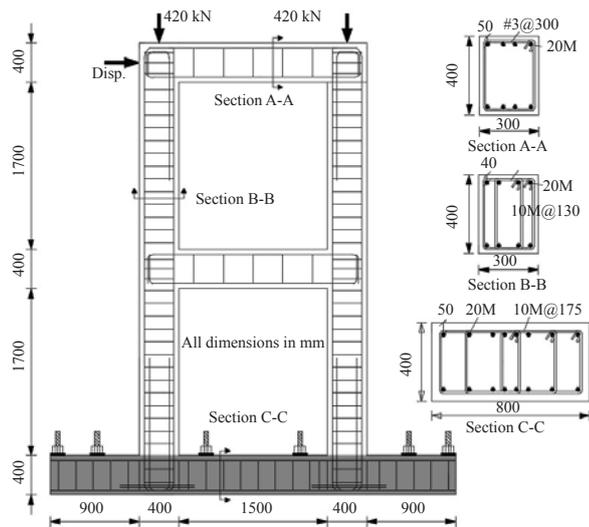

Fig. 15 Details of Duong frame (dimensions in mm)

4.2 Physical specimen of hybrid test

For the hybrid simulation test, a 1/3.23-scale representation of the lower storey beam, the most critical member of the frame, was constructed. Details of the model materials are presented in Section 3.2. A similar formwork to that prepared for the column specimen described in Section 3.3 was constructed. The formwork included two reinforced concrete end blocks with dimensions of 250 mm × 93 mm × 70 mm and a test region representing the scaled beam with dimensions of 464 mm × 124 mm × 93 mm. The end block was heavily reinforced with three D4 closed stirrups, four 12.7 mm diameter threaded rods, two 25.4 mm thick steel clamp plates, and a 12.7 mm thick steel end plate. High strength threaded rods and bolts were used to post-tension the end blocks to the loading table and the top support beam. Fig. 16 shows details of the small-scale specimen.

The reinforcement configuration of the scaled beam was adjusted so that the yielding forces of the small-scale specimen and the large-scale beam were in correct proportion. For the longitudinal reinforcement, ten heat treated D4 bars with an average measured diameter of 5.73 mm and an average yielding strength of 413 MPa were used. For the transverse reinforcement, six 316L stainless steel wires with an average measured diameter of 3.10 mm and an average yielding strength of 411 MPa were employed. The computed yielding forces of the small-scale beam were respectively 4% and 8% higher in the longitudinal and transverse directions to those obtained from the prototype beam, and thus were deemed acceptable. A concrete cover thickness of 15.5 mm was used for the scaled hybrid test beam. The specimen was tested 14 days after casting the concrete. It is worth noting that, for the hybrid test, the level of axial force in the beam was relatively small (i.e., maximum axial force was 17% of the maximum shear force).

Table 2 Material properties of Duong frame

Concrete		
f'_c (MPa)	ε_o (× 10⁻³)	Max Agg. Size (mm)
43	2.31	10

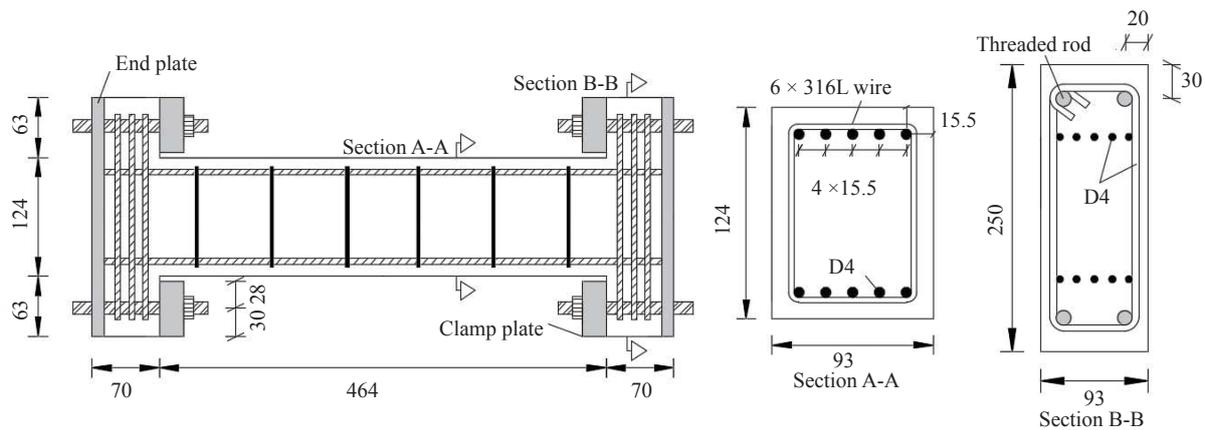| Reinforcement							
Bar Size	Diameter (mm)	Area (mm²)	f_y (MPa)	f_u (MPa)	E (MPa)	E_{sh} (MPa)	ε_{sh} (× 10⁻³)
10M	10	100	455	583	192,400	1195	22.8
20M	20	300	447	603	198,400	1372	17.1
US #3	9.5	71	506	615	210,000	1025	28.3

Fig. 16 Details of small-scale beam specimen (dimensions in millimeters)

4.3 Numerical models

For the mixed-type analysis, the shear-critical beams were modelled in VecTor2 using membrane elements, while the remainder of the frame was modelled in VecTor5 with layered beam elements. The VecTor2 sub-model comprised of 820 concrete rectangular elements and 164 steel truss elements. The longitudinal reinforcement was represented discretely using truss elements, and the transverse reinforcement was uniformly distributed over the height of the section. The VecTor5 sub-model, which represented non-critical members of the frame, contained 56 fibre beam elements each divided into 30 concrete layers. A stiffer section was used for the joint panels to avoid premature failure. A constant nodal force of 420 kN was imposed in the downward direction at the top node of each column. Also, the horizontal displacement of the top left corner node was controlled in a reversed cyclic manner with increments of 0.1 mm. The post-tensioned bolts that provided a fixed support for the frame base were modelled by restraining the corresponding nodes in the translational and rotational directions. For the hybrid simulation test, the numerical substructure was identical to that used for the mixed-type analysis except that the first-storey beam was replaced with the test specimen. Figure 17 shows details of the hybrid simulation numerical model.

4.4 Results and discussion

The load-deflection response of hybrid simulation was compared against that obtained from the full-frame test and mixed-type analysis in Fig. 18. In general, the hybrid simulation response correlated well with the mixed-type analysis results and was comparable to the full-frame test data. Both the hybrid simulation and the mixed-type analysis overestimated the stiffness and strength of the frame in the forward loading cycle. This was mainly attributed to the effects of the drying shrinkage that occurred in the full-frame specimen during the nine months between casting the concrete
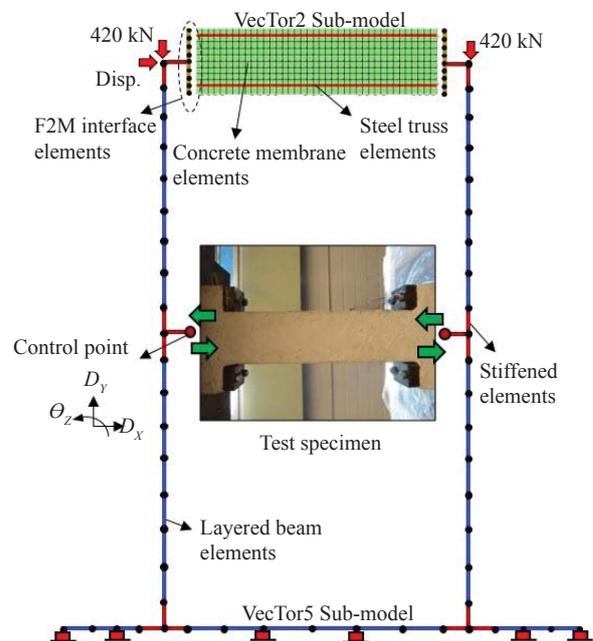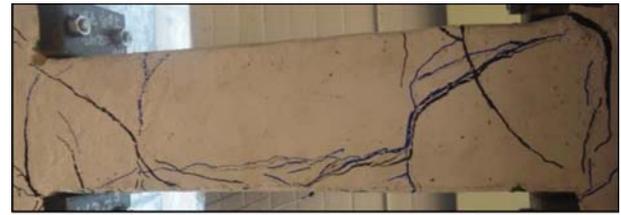

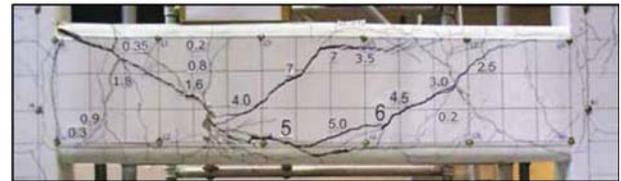**Fig. 17 Numerical and physical substructures for hybrid simulation**

and testing the specimen. Conversely, the small-scale specimen was not influenced by shrinkage effects because the time between the casting and testing was short (14 days) and also because the beam specimen was not restrained by the columns as they were numerically modelled. To be consistent with the physical component, the shrinkage effects were not considered in the hybrid simulation numerical component nor in the mixed-type analysis. Sadeghian and Vecchio (2016) analyzed the same structure with the inclusion of shrinkage strains which resulted in a better estimation of stiffness and ultimate strength. Furthermore, the stiffness and strength of the initial loading cycles were lower for the hybrid simulation compared to the mixed-type analysis which was reasonable given that the microconcrete exhibited a softer response than the prototype concrete at the material-level.

As seen in Fig. 18, both the hybrid simulation and the analysis overestimated the pinching effect compared to the full-frame test. For the full-frame test, the longitudinal reinforcement in the beam reached the yielding stress (447 MPa) at a lateral displacement of 25.5 mm. However, the maximum stress computed by the analysis was marginally below the yielding stress (434 MPa). Thus due to the yielding of the longitudinal reinforcement in the beams, the full-frame test experienced higher plastic strains and greater permanent damage than in the analysis, resulting in a less pinched hysteretic response. A similar argument can be made for the hybrid simulation since the second-storey beam was numerically modelled. It is worth noting that the hybrid test resulted in slightly better simulation of pinching behaviour than the analysis. In addition, the analysis computed yielding of the transverse reinforcement in the first- and second-storey beams in the forward loading cycle which closely matched with the results reported from the full-frame test. The numerical model of the hybrid simulation also led to similar stress values in the second-storey beam. For the physical component of the hybrid simulation, due to the scaled dimensions of the specimen, the strain values in the reinforcing bars and wires were not measured.
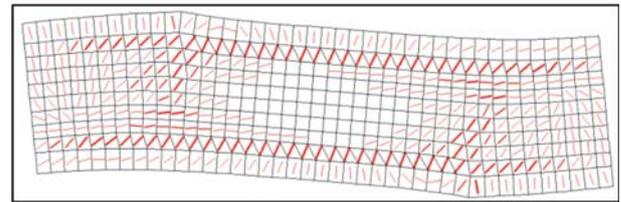
The crack patterns of the lower-storey beam obtained from the hybrid simulation, full-frame test, and finite element analysis at the peak displacement in the backward loading cycle are presented in Fig. 19. The small-scale specimen experienced two diagonal shear cracks located at each end of the specimen, which continued as a horizontal crack along the longitudinal reinforcement at the bottom of the section. Also, two flexural cracks developed at the interface of the beam and end blocks. Although the crack pattern was similar with that exhibited by the prototype beam and the analysis, the following differences were observed: 1) the shear crack width was smaller in the small-scale specimen, 2) the shear crack developed at the mid-span of the prototype beam was not found in the small-scale

(a) Scaled hybrid test beam specimen

(b) Prototype beam specimen

(c) Mixed-Type Analysis (magnification factor: 10)

Fig. 19   Crack pattern of Duong frame first-storey beam at peak displacement of backward cycle

specimen, and 3) the prototype specimen experienced several flexural cracks near the interface of the beam and column, while the flexural cracks in the small-scale specimen were more concentrated. These discrepancies were primarily the consequence of the scaling effects as it have been shown that the small-scale tests experience shear strength degradation in later load stages with a fewer number of cracks compared to the large-scale tests (see Section 1).

While the global behaviour including the load-deflection response and crack pattern of the small-scale hybrid test agreed well with that of the large-scale full-frame specimen, parameters such as scaling effects, the difference between boundary conditions, and the accuracy of the numerical model can influence other aspects of the structural behaviour particularly at the local-level. Therefore, caution must be taken when drawing conclusions regarding results of small-scale hybrid tests.

Figure 20(a) shows comparison between the command displacements (CMD) and displacements measured by the actuators LVDTs and 3D scanner (LVDT MSD and EXT MSD, respectively) at the control point of the small-scale beam specimen. The displacements represent relative deformations between the two ends of the beam. The 3D scanner measurements were performed manually at approximately every 100 load stages. The level of errors between the command displacements and displacements measured by the actuators LVDTs is
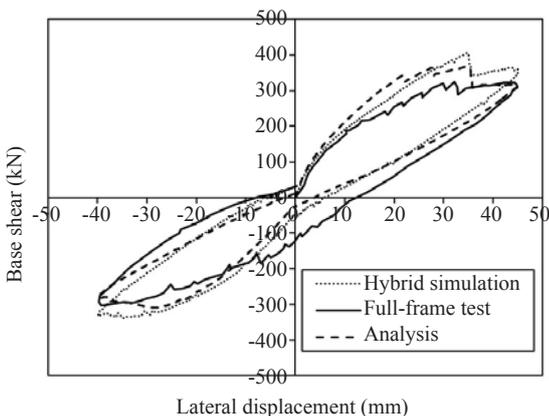

Fig. 18   Comparison of the load-deflection responses for the Duong frame

(a) Relative displacement components
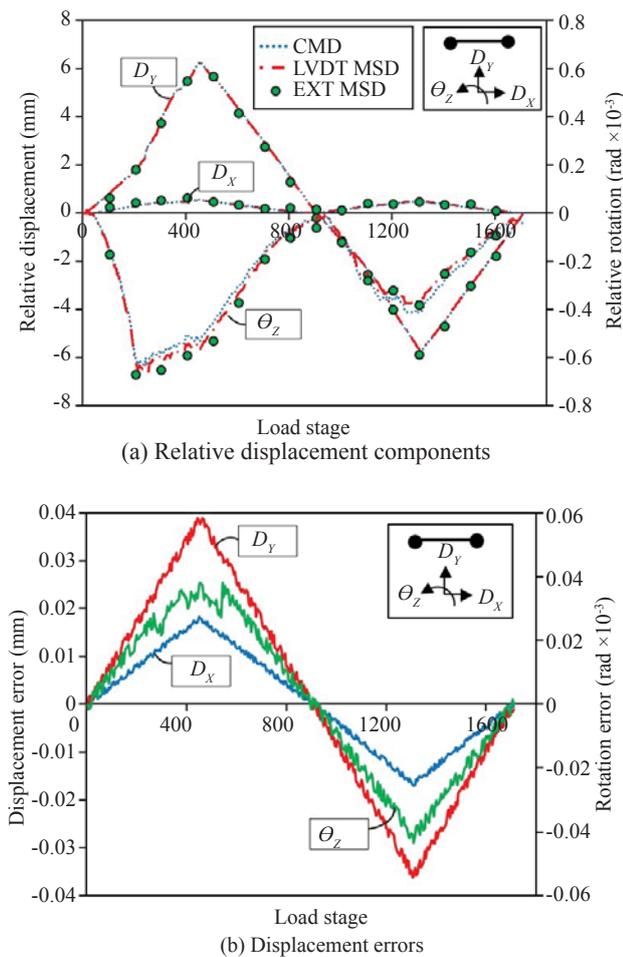

(b) Displacement errors

Fig. 20 Comparison between command and measured displacements at control point of scaled hybrid beam specimen

shown in Fig. 20(b). It can be seen that the command and measured translational and rotational displacements matched well and the level of errors were acceptable.

According to the LED measurements, no relative movement was observed at the support locations. Also, the external displacement measurements at the control point of the specimen accurately matched with the actuators LVDTs measurements.

In conclusion, based on the load-deflection response, crack pattern of the physical substructure, and stress values of the numerical substructure, the small-scale hybrid simulation found significant shear degradation in the beams due to the inadequate shear reinforcement which was consistent with the results reported from the full-frame test.

5   Summary and conclusions

The multi-scale framework, Cyrus, was enhanced with hybrid simulation capability enabling the integration of physical test specimens with numerical models. To evaluate the performance of the hybrid simulation framework and investigate the behaviour of model reinforced concrete members, particularly under shear loads, a small-scale testing program was carried out using multi-axial hydraulic testing equipment. Material tests were performed to properly simulate the behaviour of concrete and reinforcement in small-scale. The hybrid test results were compared against those obtained from stand-alone numerical models and a previously conducted large-scale test. The material and structural test results support the following conclusions:

1. The results obtained from external LED displacement measurements and steel frame tests verified the accuracy of the proposed hybrid simulation system; the displacements and reactions at the control point of the specimen were accurately measured.

2. The material test results showed that with the use of a proper mix design for the microconcrete and a heat treatment process for the reinforcing bars, the stress-strain response of the prototype material can be adequately simulated in small-scale. To control the excessive compressive strains of the microconcrete, adjusting the *W/C* ratio, limiting the minimum size of aggregate, modifying the aggregate gradation, and considering the maturity level of the mix was found to be necessary.

3. The hybrid test results of the reinforced concrete frames demonstrated that, if precautions are taken in preparing the model materials and constructing the scale specimen, small-scale hybrid simulation can represent the behaviour of the prototype reinforced concrete structure reasonably well. In particular, the failure mode, load-deflection response, and crack pattern were accurately captured. However, for all three specimens, the small-scale test led to a fewer number of cracks with a more concentrated damage zone compared to the prototype specimen and finite element analysis. Also, due to scaling effects, shear strength degradation occurred in later load stages, resulting in smaller final crack widths in the shear-critical small-scale specimens. These discrepancies between the small-scale and prototype behaviours were considered acceptable as most previous small-scale studies reported similar findings.

4. The mixed-type modelling approach was found to be an effective and efficient method for numerical components of the hybrid simulations. It eliminates deficiencies associated with the frame-type analysis methods and enables capture of the detailed response behaviour of the critical members of the numerical model. For example, with the Duong frame hybrid simulation, the mixed-type model accurately captured the shear related-mechanisms in the second-storey beam, while the remainder of the numerical components were modelled in a frame-type analysis program.

5. The main motivation behind the Duong frame large-scale test was to investigate the behaviour of an

existing cement preheater tower located in El Salvador which had several deficiencies including inadequate shear reinforcement in the beams. In this study, the same structure was successfully tested in a hybrid simulation manner with a small-scale model of the lower-storey beam representing the physical component. Compared to the full-frame test, the hybrid test required significantly less preparation time, labor, and laboratory space. Although the promising results of this study demonstrated the effectiveness of the small-scale hybrid simulation as an affordable testing method in assessing the general behaviour of a real-world structure, more test data are required to further investigate the application of hybrid simulation to model test specimens. Specifically, measuring the strain values in the small-scale specimen to determine potential yielding of the reinforcing bars and crushing of the microconcrete can greatly benefit the assessment process. Due to the above-mentioned limitations in small-scale testing, care should be taken in interpreting the results and drawing conclusions regarding the behaviour of similar real-size structures.

6. Conducting hybrid simulations in a quasi-static manner (i.e., static cyclic loading) enables the determination of important parameters such as damage type, ductility, and energy dissipation which can be used to evaluate the performance of a structure during an earthquake. To consider dynamic effects (e.g., inertia, mass, and damping) in the hybrid test, the dynamics loads can be applied on the VecTor2 and VecTor5 numerical modules and they can compute the equivalent forms of the stiffness matrix and force vector which contain dynamic effects. Cyrus combines the equivalent stiffness matrix and force vector with restoring forces and initial stiffness matrix obtained from the physical module and performs the hybrid simulation. To apply the dynamic loads directly through Cyrus, a time integration scheme is required. The implementation of a generalized time integration method into the simulation framework is currently under development.

7. By implementing a time integration method into the framework, a similar hybrid simulation configuration can be used to assess the performance of a structure under seismic loads and consider dynamic effects such as inertia, mass, and damping.

References

Collins MP and Kuchma D (1999), "How Safe Are Our Large, Lightly Reinforced Concrete Beams, Slabs, and Footings?" *ACI Structural Journal*, **96**(4): 482–490.

Collins MP, Vecchio FJ and Selby RG (1997), "The Failure of an Offshore Platform," *Canadian Journal of Civil Engineering,* **24**(3): 460–470.

Comité Euro-International du Béton (1990), *CEB-FIP Model Code,* Thomas Telford, London, UK.

CSA Committee A23.3 (2014), *Design of Concrete Structures*, Canadian Standard Association, Rexdale, Ontario, Canada, 297 pp.

Duong KV, Sheikh SA and Vecchio FJ (2007), "Seismic Behavior of Shear-Critical Reinforced Concrete Frame: Experimental Investigation," *ACI Structural Journal,* **104**(3): 303–310.

Gencturk B and Hosseini F (2015), "Evaluation of Reinforced Concrete and Reinforced Engineered Cementitious Composite (ECC) Members and Structures using Small-Scale Testing," *Canadian Journal of Civil Engineering*, **42**(3): 164–177.

Ghorbani-Renani I, Velev N, Tremblay R, Palermo D, Massicotte B and Léger P (2009), "Modeling and Testing Influence of Scaling Effects on Inelastic Response of Shear Walls," *ACI Structural Journal*, **106**(3): 358–367.

Guner S and Vecchio FJ (2011), "Analysis of Shear-Critical Reinforced Concrete Plane Frame Elements under Cyclic Loading," *Journal of Structural Engineering*, ASCE*,* **137**(8): 834–843.

Harris HG and Sabnis GM (1999), *Structural Modeling and Experimental Techniques*, CRC Press, Boca Raton, USA.

Hognestad E (1951), "A Study of Combined Bending and Axial Load in Reinforced Concrete Members," *Technical Report.* No. 399, University of Illinois at Urbana Champaign, USA.

Holub CJ (2009), *Interaction of Variable Axial Load and Shear Effects in RC Bridges,* PhD Thesis, University of Illinois at Urbana Champaign, Illinois, USA, 480 pp.

Huang X, Sadeghian V and Kwon O (2015), "Development of Integrated Framework for Distributed Multi-Platform Simulation," *6th International Conference on Advances in Experimental Structural Engineering*, Illinois, USA.

Kim W, El-Attar A and White RN (1988), "Small-Scale Modelling Techniques for Reinforced Concrete Structures Subjected to Seismic Loads," *Technical Report,* No. NCEER-88-0041, University of Cornell, New York.

Lu Y, Vintzileou E, Zhang G-F and Tassios TP (1999), "Reinforced Concrete Scaled Columns under Cyclic Actions," *Soil Dynamics and Earthquake Engineering*, **18**(2): 151–167.

McDaniel C, Benzoni G and Priestley N (1997), "Scale Effects on the Shear Strength of Circular Reinforced Concrete Columns," *Technical Report*, No. SSRP-97/02, University of California, San Diego.

Nakata N, Spencer BF and Elnashai AS (2010), "Sensitivity-Based External Calibration of Multiaxial Loading System," *Journal of Engineering Mechanics*, **136**(2): 189–198.

Noor FA and Wijayasri S (1982), "Modeling the Stress-Strain Relationship of Structural Concrete," *Magazine*

of Concrete Research, **34**(118): 25–34.

Ohtaki T (2000), "An Experimental Study on Scale Effects in Shear Failure of Reinforced Concrete Columns," *12th World Conference on Earthquake Engineering*, Auckland, New Zealand.

Sadeghian V (2017), *A Framework for Multi-Platform Analytical and Experimental Simulations of Reinforced Concrete Structures*, PhD Thesis, University of Toronto, Toronto, Canada, 321 pp.

Sadeghian V, Vecchio FJ (2016), "Application of Multi-scale Modelling on Large Shear-Critical Reinforced Concrete Structural Systems Repaired with FRP Sheets," *Durability of Repairs Special Issue, Innovations in Corrosion and Materials Science Journal,* **6**(2): 106–114.

Sadeghian V, Vecchio FJ and Kwon O-S (accepted for publication in 2017), "Modelling Beam-Membrane Interface in Reinforced Concrete Frames," *ACI Structural Journal*.

Sadeghian V, Vecchio FJ and Kwon O-S (under review) "A Multi-Platform Framework for Analytical and Experimental Simulation of Reinforced Concrete Structures," *ACI Structural Journal*.

Saouma V, Haussmann G, Kang D-H and Ghannoum W (2014), "Real-Time Hybrid Simulation of a Nonductile Reinforced Concrete Frame," *Journal of Structural Engineering,* ASCE, **140**(2).

Shioya T (1989), "Shear Properties of Large Reinforced Concrete Members," *Special Report*, No. 25, Institute of Technology, Shimizu Corp., 198 pp.

Vecchio FJ (2002), "Contribution of NLFEA to the Evaluation of Two Structural Concrete Failures," *Journal of Performance of Constructed Facilities*, ASCE, **16**(3): 110–115.

Wallace BJ and Krawinkler H (1985), "Small-Scale Model Experimentation on R/C Assemblies, US-Japan Research Program," *Technical Report,* No. 74, University of Stanford, USA.

Wong PS, Vecchio FJ and Trommels H (2013), *VecTor2 User's Manual,* University of Toronto, Toronto, Canada, 347 pp.

Zhan H and Kwon O-S (2015), "Actuator Controller Interface Program for Pseudodynamic Hybrid Simulation," *15th Advances in Structural Engineering and Mechanics*, Incheon, Korea.